PAPER • OPEN ACCESS

EMC3-EIRENE simulation of first wall recycling fluxes in W7-X with relation to H-alpha measurements

EMC3-EIRENE simulation of first wall recycling fluxes in W7-X with relation to H-alpha measurements

V R Winters[1], F Reimold[1], R König[1], M Krychowiak[1], T Romba[1], C Biedermann[1], S Bozhenkov[1], P Drewelow[1], M Endler[1], Y Feng[1], H Frerichs[2], G Fuchert[1], J Geiger[1], Y Gao[1], J H Harris[3], M Jakubowski[1], P Kornejew[1], T Kremeyer[2], H Niemann[1], E Pasch[1], A Puig-Sitjes[1], G Schlisio[1], E R Scott[1,2], G A Wurden[4] and the W7-X Team[5]

[1] Max-Planck-Institut für Plasmaphysik, D-17491 Greifswald, Germany
[2] University of Wisconsin—Madison, Madison, WI 53706, United States of America
[3] Oak Ridge National Laboratory, Oak Ridge, TN 37830, United States of America
[4] Los Alamos National Laboratory, Los Alamos, NM 87545, United States of America

E-mail: victoria.winters@ipp.mpg.de

CrossMark

Abstract

In the Wendelstein 7-X stellarator, the main locations of particle sources are expected to be the carbon divertors, baffles and graphite heat shield first wall. In this paper, the heat shield is implemented in EMC3-EIRENE to understand the expected areas and magnitudes of the recycling flux to this component. It is found that in the simulation the heat shield is not a significant source of recycling neutrals. The areas of simulated recycling flux are shown to correlate well with footprints of plasma-wetting seen in post-experimental campaign in-vessel inspection photos. EMC3-EIRENE reconstruction of line-integrated H-alpha measurements at the heat shield indicate that the majority of emission does not come from local recycling neutrals. Rather, the H-alpha signals at the heat shield are dominated by ionization of neutrals which have leaked from the divertor/baffle region into the midplane. The magnitude of the H-alpha line emission from the synthetic reconstruction is consistent with the experiment, indicating that a large overestimation of heat shield recycling would occur if these measurements were assumed to be from local recycling sources. In the future, it may be possible to obtain some information of local recycling from the heat shield since it was found that the majority of the recycling flux occurs on two well-localized areas.

Keywords: EMC3-EIRENE, recycling, stellarator, W7-X, spectroscopy, SOL

(Some figures may appear in colour only in the online journal)

1. Introduction

The particle balance, in part obtained by hydrogen recycling measurements on the plasma-facing components (PFCs), is important to understand wall retention and fueling in fusion devices [1]. In the Wendelstein 7-X (W7-X) stellarator, it is expected that the main sources of hydrogen recycling come from the carbon PFCs (namely the divertors, baffles and heat shield first wall). Although the divertors are expected to be the
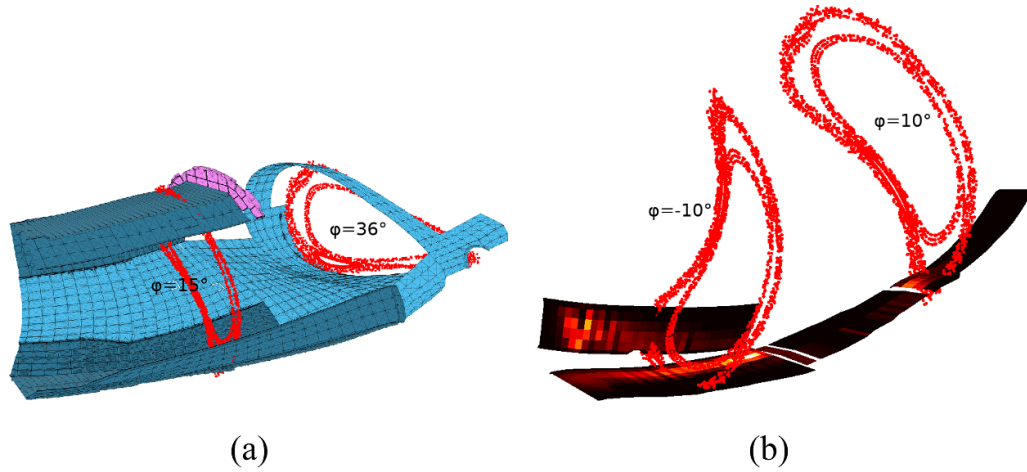
Figure 1. (a) The carbon PFCs in W7-X for one half module. The divertor and baffle are plotted in dark blue. The heat shield is plotted in blue. The region to the right of the toroidal closure, plotted in purple, is not well covered by spectroscopic diagnostics. (b) The intersection of the magnetic islands at the main horizontal and vertical target as well as at the high iota tail, forming the main plasma strike line in the standard divertor configuration.

region that has the largest recycling flux densities, the large surface area of the heat shield has the potential to make it a significant contributor in the recycling source, even for lower flux densities. However, to date no detailed investigation has been performed to determine the expected total recycling source and locations of interaction on this component.

Currently, the heat shield recycling source is monitored with a set of visible cameras [2] and Filterscopes [3] outfitted with H-alpha (656.3 nm, 2 nm FWHM) filters. The H-alpha emission may originate from multiple atomic/molecular processes which includes [4]:

$$H_2 + e^- \rightarrow H + H^* + e^- \rightarrow H + H + e^- + H_\alpha$$
Dissociative Excitation
$$H_2 + e^- \rightarrow H^+ + H^* + 2e^- \rightarrow H^+ + H + 2e^- + H_\alpha$$
Dissociative Ionization
$$H_2^+ + e^- \rightarrow H^+ + H^* + e^- \rightarrow H^+ + H + e^- + H_\alpha$$
Dissociative Excitation
$$H_2^+ + e^- \rightarrow H^* + H \rightarrow H + H + H_\alpha$$
Dissociative Recombination
$$H + e^- \rightarrow H^* + e^- \rightarrow H + e^- + H_\alpha$$
Atomic Excitation
$$H^+ + e^- \rightarrow H^* \rightarrow H + H_\alpha$$
Radiative Recombination.
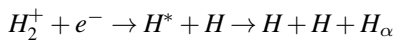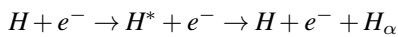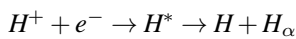
The total emission from these processes is measured by the spectroscopic diagnostics. This total H-alpha emission, combined with hydrogen photon efficiencies [5], provides the ionization source of hydrogen particles and often a direct relation to the local recycling flux is assumed. However, the H-alpha emission measured by these diagnostics is line-integrated. Therefore, it is difficult to validate, particularly for the heat shield where the recycling fluxes are expected to be low, the assumption that the local recycling source is the dominant contributor to the neutral ionization source.

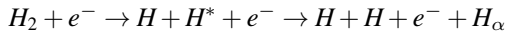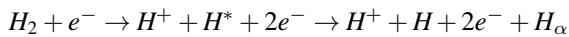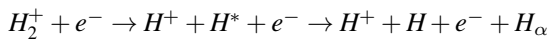This paper aims both to investigate locations and magnitudes of plasma-wetting to the first wall using 3D modeling from EMC3-EIRENE [6, 7] and to use the insight from these results for diagnostic sight line adjustment and interpretation for the error-field free standard divertor magnetic field configuration. In the following section, a description of the carbon PFCs and the viewing areas of the current H-alpha spectroscopic lines of sight is provided. Section 3 details the EMC3-EIRENE simulation of the heat shield recycling fluxes. The total contribution of the heat shield to the total recycling flux is given and the areas of main heat shield recycling are compared to the experiment. In the final section, the synthetic diagnostic capability of EMC3-EIRENE, which has been tested and used on several 3D devices [8–12], is used to determine whether the assumption that the local recycling flux dominates the line integrated H-alpha signal is valid for measurements at the heat shield. The relation of these results to the current understanding and set-up of the experiments will be provided at the end.

2. The carbon PFCs of W7-X

The carbon PFCs in W7-X for one half-module are visualized in figure 1(a), where the divertors and baffles are plotted in dark blue, the toroidal closure plotted in purple, and the heat shield in light blue. The total surface areas of each component type are 25, 33 and 52 m^2, respectively [13]. For visualization of the main plasma strike line, the particle flux pattern on the lower divertor, which spans one full module, is plotted in figure 1(b).

In the standard magnetic field configuration, the plasma strike line is located at the main horizontal and vertical divertor targets as plotted in figure 1(b). At the location of primary strike line at the divertors, a Poincaré plot (at toroidal angle $\phi = 10°$ in (a) and $\phi = -10°$ in (b)) in red visualizes the intersection of the islands at the target. The other half of the divertor target, at the bottom of figure 1(a) is labeled as the 'high iota'

portion of the divertor target. In the standard divertor config-
uration, there is a small region of plasma surface interaction
on this portion of the divertor, visualized in figure 1(b) with
a Poincaré plot at $\phi = 15°$. On the far right side of the figure
is the triangular plane of the plasma vessel, where the heat
shield covers nearly the entire poloidal region of the first wall.
Here, another Poincaré plot ($\phi = 36°$) in red is visualized. The
heat shield design follows the shape of the plasma contour on
the inboard side of the vessel. Because the dedicated H-alpha
spectroscopic diagnostics were primarily focused on measur-
ing the particle fluxes from the baffle and divertor regions,
the heat shield area beyond the divertor from about $\phi = 19$
(the location of the toroidal closure) to $\phi = 36°$ is not well
diagnosed.

## 3. EMC3-EIRENE modeling of the heat shield

The 3D Monte Carlo plasma edge code package EMC3-
EIRENE [6, 7] solves a set of Braginskii plasma fluid
equations in steady-state, with neutral particle sources and
interaction with neutrals solved kinetically. Both the EMC3
(fluid plasma) and EIRENE (kinetic neutral) portions of the
code are well-documented and can be found in various [7, 14].

The EMC3-EIRENE simulation presented here utilizes the
standard magnetic field configuration, which was used for the
largest amount of plasma seconds in the last operational cam-
paign [15]. The simulation assumes vacuum field, and thus
no plasma response is taken into account. Additionally, the
ideal magnetic field configuration without error fields was
used [16]. One half-module (0°–36° toroidally) is simulated in
the code, with stellarator symmetry assumed and drift effects
not included. The input heating power was set to be 4.5 MW
with a separatrix density of 1×10^{19} m^{-3}, which was rel-
atively typical for low density plasma operation. The recy-
cling source is the only particle source in the simulation, with
no particle sinks and therefore the upstream density sets the
total recycling flux to achieve particle balance. The radiated
power is kept to 16% of the total input heating power, with
the radiation coming from chemically-sputtered carbon impur-
ities. The anomalous perpendicular diffusion coefficient was
scanned from $D = 1$ m^2 s^{-1} to $D = 5$ m^2 s^{-1} to determine the
sensitivity of the magnitude of the heat shield fluxes to the
diffusion coefficient and to isolate effects of pure particle dif-
fusion the perpendicular heat diffusivity coefficient was kept
constant at $\chi = 3$ m^2 s^{-1}.

As this paper aims to determine order-of-magnitude fluxes,
no detailed match to any particular experimental discharge is
used. However, the input parameters were very similar to those
of program 20180920.013, which also had an input heating
power of 4.5 MW, separatrix density of $\approx 1 \times 10^{19}$ m^{-3} with
a radiated power fraction of 16%. All experimental compar-
isons in this paper are based off of experimental data from
this program. Although EMC3-EIRENE only models the SOL
and the edge of the confined plasma, plasma electron density
and temperature profiles and ion temperature profiles can be
used as input to the code to model core neutral transport with
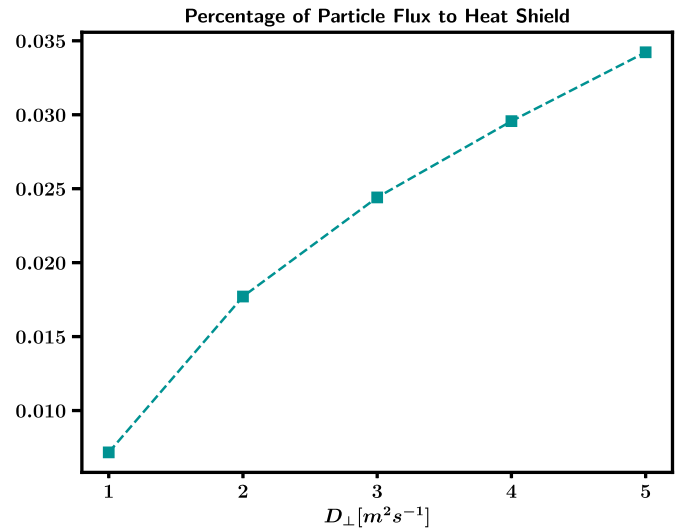
Figure 2. The percentage of the total recycling flux which occurs on
the first wall as a function of the perpendicular diffusion coefficient.
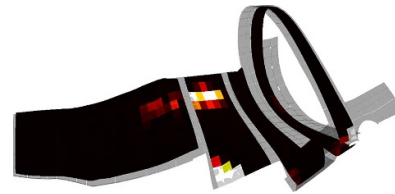
Figure 3. Locations of particle flux on the heat shield as simulated
by EMC3-EIRENE.

EIRENE. The core profiles inputted into these simulations
were based off of Thomson scattering profiles from program
20180920.013 [17]. It should be noted that although error-
field correction was applied for this experimental program,
full error-field compensation has not yet been possible exper-
imentally and still results in some asymmetry of the heat flux
to different divertors [16] which is not accounted for in the
simulation.

For a global picture of how the heat shield contributes to the
total recycling source, the percentage of the total recycling flux
which occurs on the first wall as a function of the perpendicu-
lar diffusion coefficient is plotted in figure 2. As the diffusion
coefficient is increased, the percentage of the total recycling
flux to the heat shield also increases. However, even among
high values of diffusion coefficient, the recycling flux from
the heat shield remains below 4% of the total. For typical dif-
fusion coefficients used for W7-X simulations ($D = 1$ m^2 s^{-1})
the recycling flux from the heat shield is <1%. Therefore, the
simulation results indicate that the heat shield does not play
a large role in the overall particle balance. To validate these
results, the distribution of the particle flux on the surface is
first compared to the experiment. Then, more detailed meas-
urements with regard to H-alpha will be discussed in the next
section.

The locations of all expected plasma-interaction areas
on the heat shield are plotted in figure 3. Although the
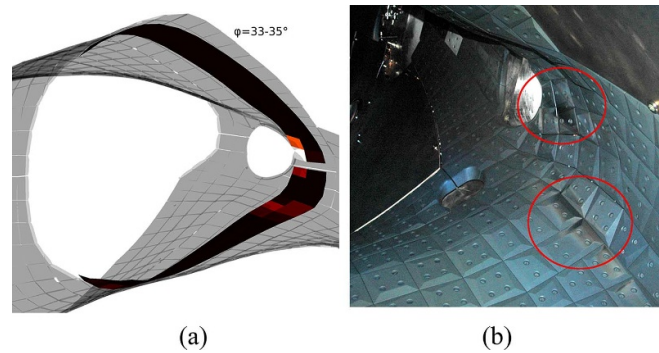
Figure 4. (a) EMC3-EIRENE simulation of the heat shield interaction zone in the triangular plane from $33°$ to $35°$ toroidally. (b) In-vessel inspection photo of the heat shield in the same location. The interaction area is marked by discoloration of the graphite tiles. The loads locations, circled in red, match qualitatively to the simulation.
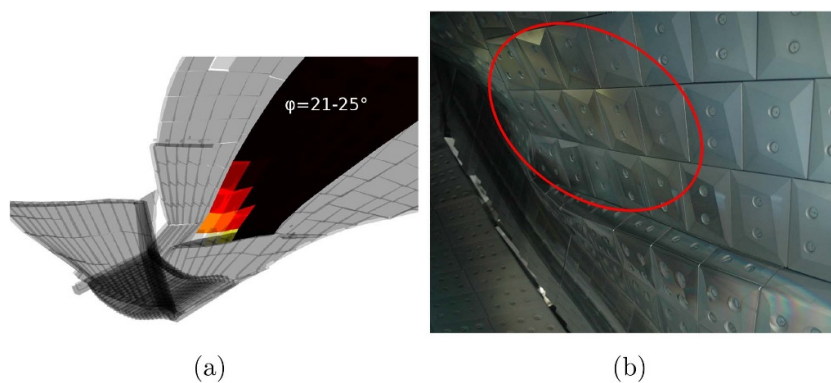
Figure 5. (a) EMC3-EIRENE simulation of heat shield load near the high iota tail, from $21°$ to $25°$ toroidally. (b) In-vessel inspection photo of the heat shield in the same location. The interaction area is marked by discoloration of the graphite tiles. The loads location, circled in red matches qualitatively to the location EMC3-EIRENE.

components appear on the plot as separated, they are all connected in the simulation such that no neutrals can leak between the components. The magnitude of the total particle flux to the heat shield increases with the perpendicular diffusion coefficient but the regions of expected interaction area remain approximately the same, with the percentage of the surface area receiving some plasma-wetting varying only from 16.5% to 19% across the diffusion coefficient scan. At diffusion coefficient values which are typically used in simulation ($D = 1\ \mathrm{m^2\ s^{-1}}$), there is one smaller region of plasma interaction near the outboard tip of the triangular plane, highlighted also in figure 4(a), as well as a larger area which is located above the high iota target (highlighted in figure 5(a)). The plasma-surface interaction region pictured in figure 5 represents 90% of the total recycling on the heat shield.

Unfortunately, the regions of localized recycling flux on the heat shield plotted in figure 3 are not well-covered by existing spectroscopic sight lines. These regions of expected plasma-wetting from simulation were instead compared to in-vessel inspection photos after plasma operation to test the validity of the simulation results. Although these interaction zones are the accumulated result of several different magnetic field configurations which were operated over the experimental campaign, the standard magnetic field

configuration was operated for the largest number of plasma seconds [15]. Therefore, the patterns seen on the heat shield should largely be an effect of this particular configuration. The in-vessel inspection photo corresponding to the region of expected wetted area at the triangular plane is given in figure 4(b). The regions of darkened tiles are evidence of plasma-surface interaction and correlate well to the simulation results, plotted in figure 4(a). Similarly, the in-vessel inspection photo corresponding to the region of expected PSI near the high iota tail is given in figure 5(b). The PSI region is marked by discoloration of the graphite tiles in the photo. Here too a good agreement between the simulation of this area, plotted in figure 5(a), and the experiment is seen.

4. Diagnostic line of sight comparisons with EMC3-EIRENE

One of the main diagnostics planned for observing the recycling flux from the heat shield are the Filterscopes. The Filterscope system at W7-X [18] consists of 72 filtered photomultiplier tubes in the visible range, with 18 unique lines of sight distributed around the entire machine. Among these lines of sight, 2 are of interest in this work. Their viewing
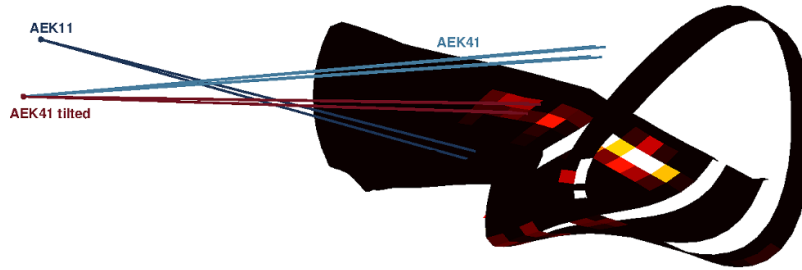
Figure 6. Filterscope view cones AEK11 and AEK41 plotted in relation to the expected particle flux load to the heat shield components. The original location of AEK41 views a baffle region (medium blue viewing area), and therefore it is proposed to tilt it downwards (maroon viewing area).

lines and areas in relation to the expected plasma loads on the heat shield are plotted in figure 6. Although each view is located in a different toroidal module (modules 1 and 4 corresponding to sight lines AEK11 and AEK41, respectively), they have been rotated for visual clarity all to the same half module, analogous to how they are modeled in EMC3-EIRENE. Both Filterscope views are nearly contained within one toroidal plane. The AEK11 center line of sight spans about 2 toroidal degrees, from 15.4 entering from the outboard side and ending at 17.6° on the inboard side. The AEK41 center line of sight spans about 1 toroidal degree, with the equivalent angles in the simulation domain of 17.4° entering from the outboard side and ending at 18.6° at the inboard side of the machine.

In the previous campaign, the majority of the Filterscope views, including AEK41, viewed the baffle rather than the heat shield. This is planned to be modified for future campaigns. The AEK11 view cone does not intersect a region of the heat shield expected to have a recycling flux, as plotted in figure 6. Although not possible in the previous experimental campaigns, it is proposed to tilt the AEK41 view cone such that it views some region of expected plasma load to compare to the measurement from AEK11. The proposed new AEK41 view cone, tilted by 6°, is also plotted in figure 6.

Even with the proposed tilted view cone of the AEK41 Filterscope channel, it is possible that the recycling flux is so low from this area of the heat shield that ionization of neutrals that are not from local recycling could have a significant effect on the signal. If that is the case, then the H-alpha measurements cannot be assumed to be a local particle flux measurement. To investigate this effect, the synthetic diagnostic module of EMC3-EIRENE [8] was used to determine the distribution of H-alpha emission along the viewing area. The diffusion coefficient used for the emission distribution calculations was $D_\perp = 1 \, \mathrm{m^2 \, s^{-1}}$, which yielded line integrated emission levels on the same order of magnitude as measured in the experiment (discussed later) for similar plasma conditions.

For the line of sight approximation used in the EMC3-EIRENE synthetic diagnostic module to be correct, each of the Filterscope view cones was split into 5×5 individual 'pixels' of the signal. Because the Filterscope diagnostic does not have any spatial resolution, the synthetic signal is the pixel-area weighted average of these contributions. The H-alpha signal

contains contributions from H atom neutrals, H_2 molecules, H_2^+ ions and H^+ ions, with emission rates supplied by the AMJUEL database [19]. It should be noted that although the H-alpha emission from radiative recombination is taken into account, radiative recombination is not used as a neutral source/sink term when computing the plasma background in EMC3-EIRENE. The distribution and composition of the H-alpha signal along one of the pixel lines of sight for the AEK41 tilted and AEK11 view cones are plotted in figures 7(a) and (b), respectively. H^+ emission is found to be negligible to the total signal in both cases. While only the neutral atoms play a significant role in the emission of the confined plasma, in the SOL both H_2 and H_2^+ contribute to the total signal level. Overall, the molecular contribution to the H-alpha signals are 10% and 15% for the AEK11 and AEK41 tilted views, respectively. The confined plasma emission in the region where only the neutral behavior on an input plasma background is modeled is 52% and 37% for the AEK11 and AEK41 tilted views, respectively.

According to simulation, there is no local recycling inside the view cone of the AEK11 Filterscope channel. Therefore, the line-integrated signal cannot originate from local recycling. Instead, the light must come from neutrals which have transported from the divertor or baffle regions into the viewing area and then ionized (leaked neutrals). This means that the signal of AEK11 is determined by the leakage from the divertor/baffle region. The synthetic line integrated signal for AEK11 is $5.5 \times 10^{18} \, \mathrm{m^{-2} \, s^{-1}}$, which is on the same order of magnitude as the tilted AEK41 view cone $(9.7 \times 10^{18} \, \mathrm{m^{-2} \, s^{-1}})$. This indicates that ionization from neutrals which leak from the divertor/baffle region to the midplane are also a significant contributor to the H-alpha signal measured in the tilted AEK41 view cone.

To better understand the percentage of the line integrated signal coming from local recycling versus neutral leakage, the graphite heat shield was removed from the simulation, but the plasma background was kept the same. Then, the neutral transport portion of the code was re-run on this plasma background. A toroidal slice at $\phi = 17°$ showing the percent change in the neutral atom and neutral molecule density, defined as $\frac{n_{withhs} - n_{nohs}}{n_{withhs}} \times 100$ is plotted in figures 8(a) and (b), respectively. In figure 8(a), toward the top of the heat shield just below the baffle, both the neutral atom and molecular density is higher with the heat shield case, whereas for the rest of the heat shield
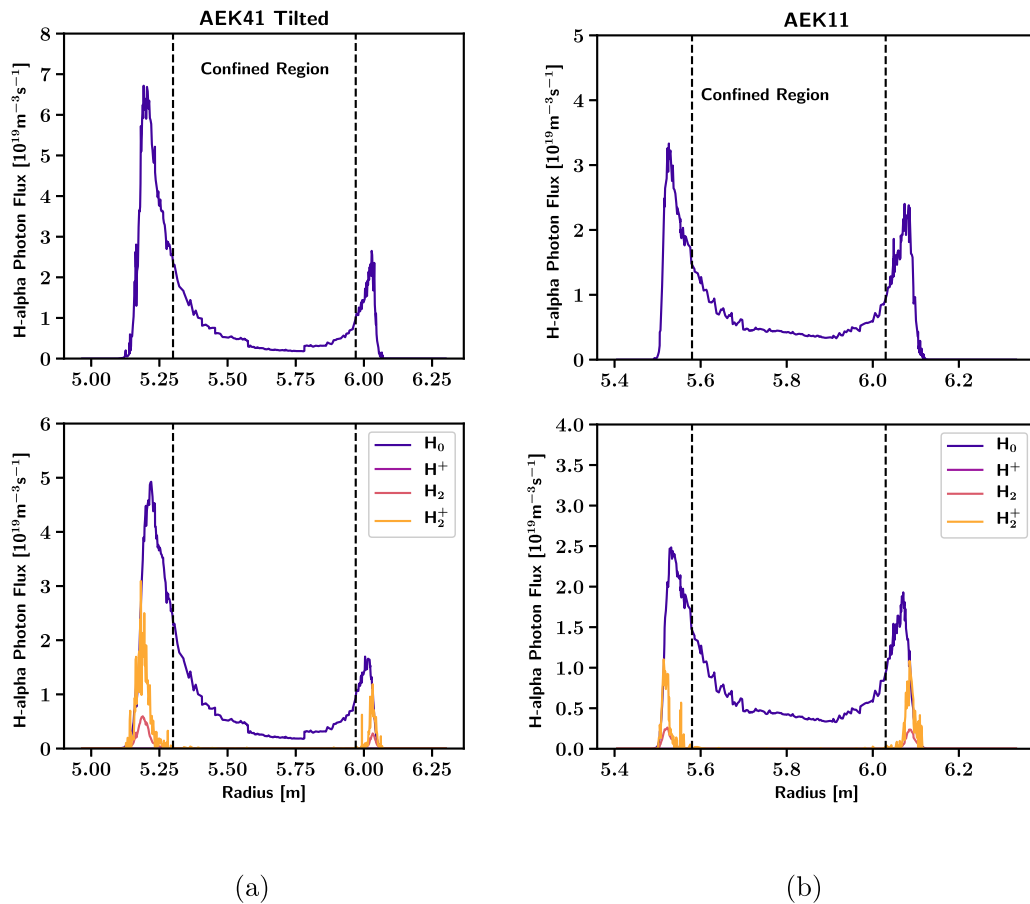
Figure 7. Distribution and composition of the H-alpha photon flux for (a) the tilted AEK41 lines of sight and (b) the AEK11 lines of sight. In both cases, the outboard side radiation makes up a significant percentage of the signal.

the atom and molecular density is somewhat lower with the heat shield. All other regions stay largely the same, with the large percentage differences of the molecules in the confined plasma due to the low statistics from the very low densities in this region. Although it could be possible that some recycling at the top portion of the heat shield could have an effect on the neutral densities measured there, it is more likely due the larger volume available for poloidally leaked neutrals to enter into the midplane without the heat shield case. As an example figures 8(c) and (d) shows the neutral atom and molecular density without the heat shield included. The colorbar is scaled such that the neutral midplane behavior is visible, which saturates the colorbar in the divertor region. Poloidal leakage from the divertor area is visualized by stripes of higher neutral density originating from the ends of the baffle. Toroidal leakage is not visualized in the plot, but is also likely the significant leakage mechanism. Because the geometry of the baffle blocks the neutrals from going in all directions, regions of lower neutral atom density appearing as 'shadows' can be seen at the midplane-facing baffle surfaces. These 'shadows' are only prominent in the neutral atom density because once the atoms are reflected off a surface they are largely reflected as molecules. When the heat shield is not included, such a region of lower neutral density also appears on the midplane-facing side of the upper inboard baffle. Including the heat shield

restricts the available volume for the leaked neutrals, manifesting in a slightly higher neutral density toward the top of the heat shield. That the other region further below the baffle shows an increase of neutral density without the heat shield indicates changes in neutral transport, rather than changes of recycling.

This indicates that the leakage from the divertor/baffle region into the midplane is the dominant factor that determines the neutral ionization source at the midplane. Although figure 8(c) indicates that poloidal leakage may be involved, there is also likely toroidal leakage out of the divertor, which is not toroidally continuous around the machine, where neutrals are then free to move to the midplane.

The conclusion that neutral leakage is the dominant player in determining the H-alpha level is also consistent with the H-alpha synthetic diagnostic reconstructions for the AEK41 tilted and AEK11 filterscope sightlines, which are plotted in figures 9(a) and (b), respectively. Both the tilted AEK41 and AEK11 lines of sight see a slight increase of the line-integrated signal without the heat shield toward the confined plasma region, indicating that any change in the signals are dominated by neutral transport rather than changes in local recycling at the heat shield. However, such changes are not able to be resolved in a line-integrated measurement.

(a)

(b)

(c)

(d)
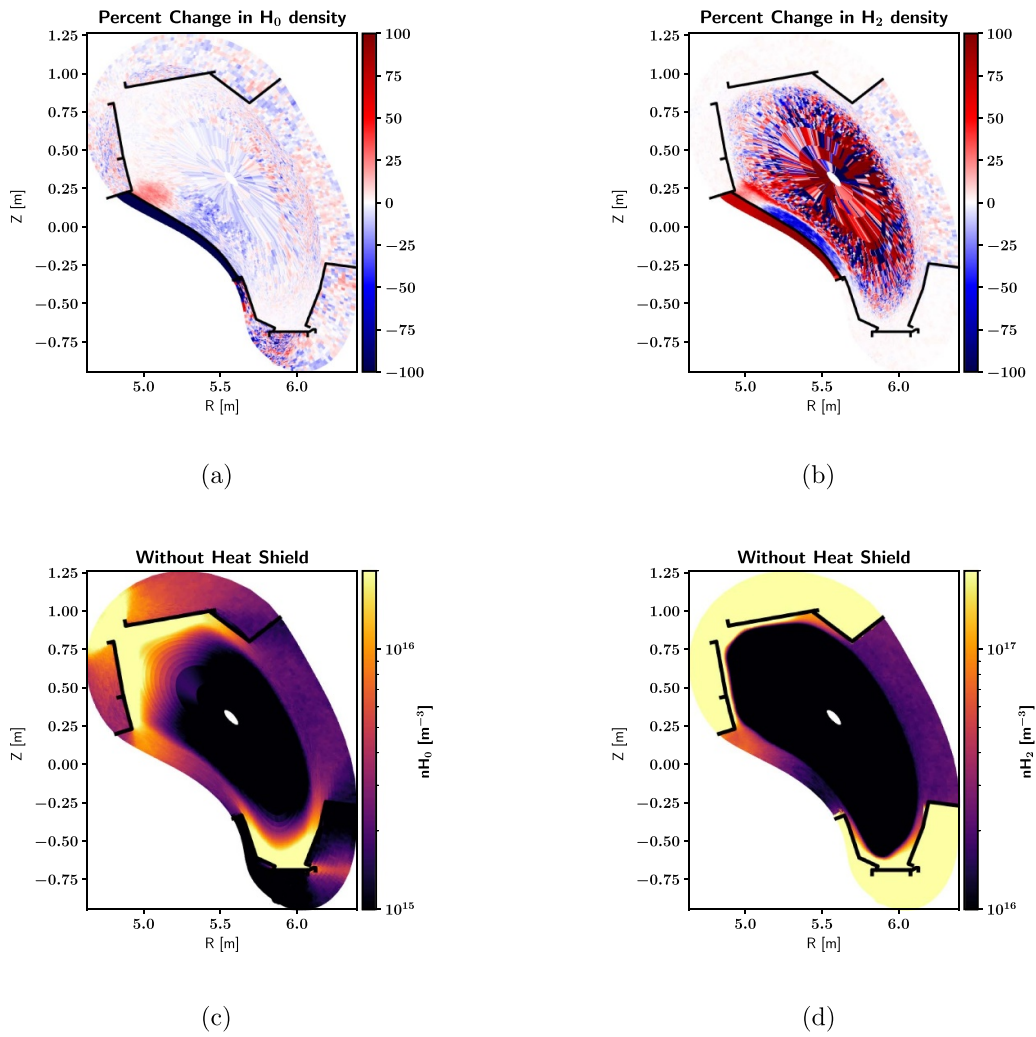
Figure 8. The percentage difference in the (a) neutral atom and (b) neutral molecular density with and without the heat shield included. The percentage difference is defined as the difference between the values with and without the heat shield included and then divided by the values with the heat shield included multiplied by 100. For both atoms and molecules, the upper region near the baffle plate has higher density with the heat shield than without. (c) The neutral atom and (d) neutral molecule density without the heat shield included.

(a)

(b)
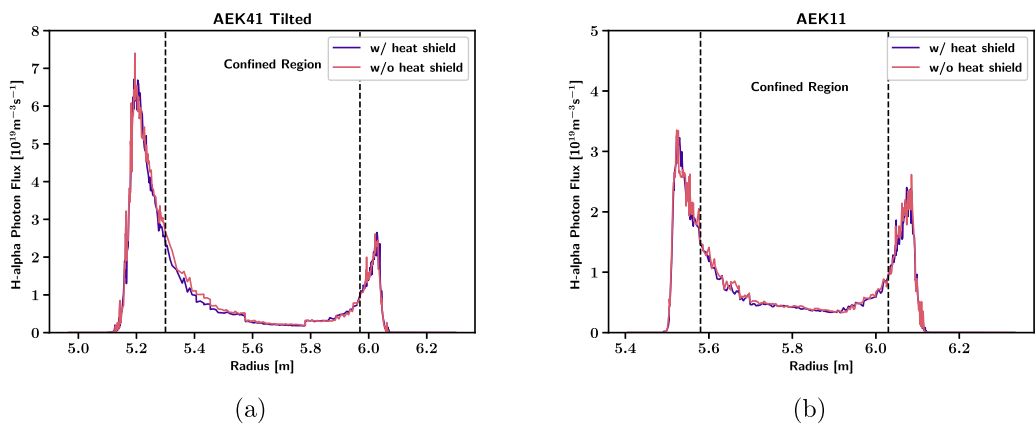
Figure 9. Comparison of the distribution of the H-alpha emission along the line of sight for the tilted AEK41 and AEK11 lines of sight with and without the heat shield included for one of the pixels from the synthetic diagnostic module from EMC3-EIRENE.
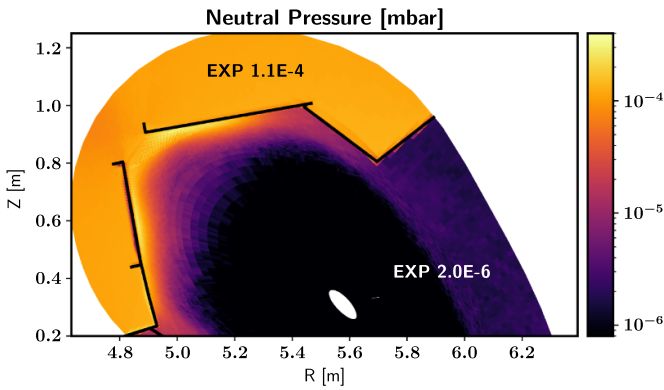
Figure 10. The neutral pressure simulated in EMC3-EIRENE. The neutral pressure measured in the experiment on the outboard midplane is written as white text in the region of the simulation corresponding to the outboard midplane. The neutral pressure measured behind the divertor in the experiment is written as black text in the region of the simulation most analogous to the measurement location.

As a qualitative check that the model is capturing the correct behavior, experimental comparisons with several diagnostics was performed. Firstly, the ratio of the neutral pressure behind the divertor to that of the outboard midplane (the neutral compression ratio) in the simulation are consistent with experimental measurement. In the $D = 1$ m^2 s^{-1} simulation, the neutral compression ratio was in the range of 40–60, which is consistent with the neutral compression ratio of 55 in experimental program 20180920.013 from pressure gauge measurements [20]. A visualization of the neutral pressure from molecules (since atoms are not believed to play a dominant role in the neutral pressure measurement [21]) in simulation compared with the pressure gauge measurements is plotted in figure 10. The neutral pressure in EMC3-EIRENE is calculated by the ideal gas law: $P_n = 1.6 \times 10^{-15} n_{H_2} T_{H_2}$ (mbar), where n_{H_2} is the molecular density in cm^{-3}, T_{H_2} is the molecular temperature in eV, with the leading numerical value being a conversion factor. The experimental measurement from the pressure gauge located behind the divertor in the pumping port is written in figure 10 in black. The experimental measurement from the pressure gauge located at the outboard midplane is written in figure 10 in white. Although the port geometry is not resolved in the EMC3-EIRENE simulation, the locations of the text on the simulation plot correspond roughly to the neutral reservoirs that each pressure gauge measures.

The magnitude of the line integrated H-alpha emission at the heat shield in simulation also agrees with the experimental measurements. Figure 11(a) visualizes an H-alpha photon flux measurement from one of the divertor visible cameras for program 20180920.013. The area of the heat shield observed by the visible cameras is labeled near the top half of the image. The divertor is distinguished by two strike lines of high photon flux: one on the vertical target (the upper stripe) and one on the horizontal target (the longer, lower stripe). On the bottom portion of the image is a stainless steel panel. The magnitude of the line-integrated signal at the heat shield location

from the divertor camera is 10^{18}–10^{19} m^{-2} s^{-1}, consistent with simulation. As a further check since dynamic range of the filtered camera is just barely within the measurement range of the heat shield signal levels, the AEK11 filterscope signal for 20180920.013 was measured to be 2.75×10^{18} photons m^{-2} s^{-1}. The divertor fluxes are at least 2 orders of magnitude higher than what is measured on the heat shield. The signal levels at both the heat shield and divertor locations are also captured to the correct order of magnitude in the simulation. A synthetic camera image from EMC3-EIRENE data of the divertor visible camera is plotted for comparison in figure 11(b). It should be noted that in the experiment, outgassing from the carbon surfaces is expected to occur which is not accounted for in the model. However, over the course of the 6 s experimental program, the temperature of the heat shield was raised only by 10 °C. It is expected that the majority of the outgassing will occur on other surfaces which receive more load and therefore heat up faster, such as the baffles or divertor. Additionally, it is expected that the neutral behavior from recycling is dominant compared to external particle sources [21] and therefore it is not likely that outgassing will comprise a significant fraction of the line-integrated H-alpha signal.

Although the large majority of the heat shield area observed by the H-alpha filtered visible camera in figure 11(a) is featureless, there is one feature marked by a white arrow in the figure. This is in a region expected to have some amount of plasma wetting according to EMC3-EIRENE, approximately in the area of the AEK41 tilted sight line. However, it is located in the same position as a reflection in the IR camera system, plotted in figure 11(c), also marked with a white arrow, which shares a line of sight with the visible camera. Therefore, it is possible that this feature is merely a reflection and not a measurement of a recycling flux. The location marked by the arrow does not see a similar region of increased H-alpha signal in the EMC3-EIRENE synthetic image since the recycling source is small compared to the leaked neutrals.

Finally, the confined neutral density in the simulation is compared to an experimental measurement for 20180920.013 using high dynamic range H-alpha spectroscopy from a subset of spectrometers used in charge exchange analysis [22]. The measurement technique was based on the analysis technique from Fujii *et al* [23]. The result is plotted in figure 12. Toward the edge channels, the neutral density simulated by EMC3-EIRENE agrees well with experimental measurements. There is some disagreement in the neutral density in the inner-most channels between experiment and simulation, with EMC3-EIRENE showing a higher neutral density. This may be due to the input plasma parameter conditions for the core neutral transport, or due to the simulation not specifically being matched for this particular experimental program. Another potential reason for the disagreement could come from the experimental side, due to the core H-alpha emission levels being close to background emission levels. However, the results from the core spectroscopy provide some confidence of the neutral behavior in simulation not only in the SOL, but also in the confined plasma.

(a)

(b)

(c)
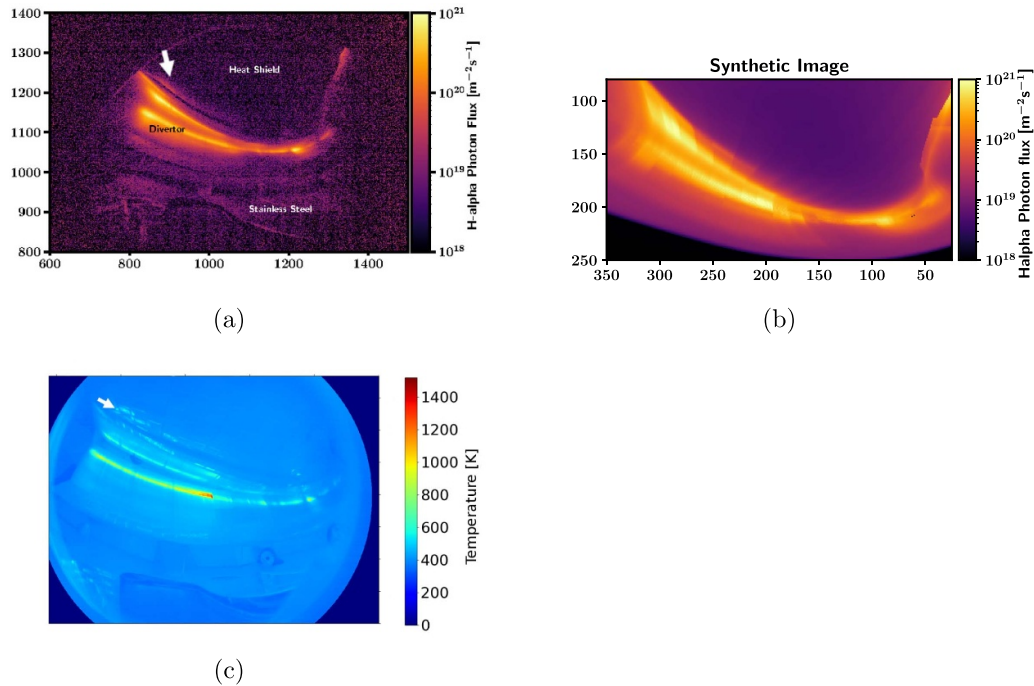
Figure 11. (a) H-alpha photon flux signals averaged over 200 ms from one of the divertor visible cameras for program 20180920.013. The heat shield is located in the upper half of the image. The divertor region, distinguished by a photon flux several orders of magnitude higher, is near the middle of the image. Stainless steel panels are seen near the bottom of the image. The region of higher photon flux near the upper right portion of the image is plasma light coming from an adjacent toroidal module. (b) A synthetic camera image generated by EMC3-EIRENE for the divertor camera. (c) IR image of the same divertor. The white arrow corresponds to a region of perceived higher temperature which is regarded instead as a reflection. This white arrow corresponds to the white arrow also shown in the photon flux image to the left.
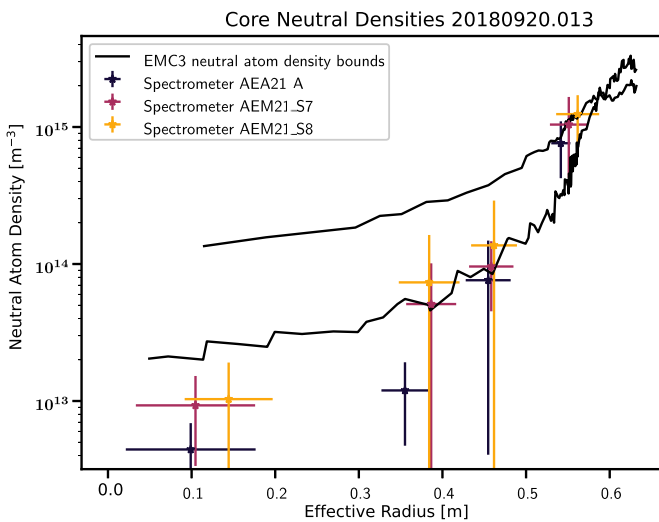
Figure 12. A comparison of the core neutral density measured in the experiment (colored symbols) with the core neutral density profiles in EMC3-EIRENE. Because the neutral density varies depending on toroidal location, an upper and lower bound are given.

5. Summary

EMC3-EIRENE was employed to study recycling fluxes from the main chamber graphite heat shield. It was found that at a separatrix density of 1×10^{19} m^{-3}, the percentage of particle flux to the heat shield was below 4% of the total recycling flux at high levels of perpendicular diffusion. In typical simulation scenarios, the particle flux to the heat shield is even lower; less than 1% of the total recycling flux at a perpendicular diffusion coefficient $D = 1$ m^2 s^{-1}, indicating that the heat shield is not a significant source of particles in simulation. The EMC3-EIRENE simulations well reproduced the pattern of plasma deposition on the heat shield as determined from post-experimental campaign in-vessel inspection photos. However, it is difficult to quantitatively compare recycling sources from the first wall experimentally, as the regions of expected interaction were not well-diagnosed by current spectroscopic viewing lines.

Without changing the current port location of the Filterscope diagnostic line of sight, a tilt of the viewing angle was proposed to attempt to measure an expected location of recycling according to simulation. Although this location of expected recycling flux is very low, it was chosen such that if a signal from the heat shield is seen, the sight line could be easily implemented for the next experimental campaign. This tilted view, along with a current view which does not measure a recycling zone, was constructed synthetically using the synthetic diagnostic module of EMC3-EIRENE. Atomic excitation was found to be the dominant contributor to the total H-alpha signal in front of the heat shield, with molecular emission only making up 10%–15% of the total signal. It was found that local recycling did not significantly contribute to the line integrated H-alpha signal. Rather, neutral ionization in front of the heat shield is dominated by neutrals which have leaked

from the divertor/baffle region to the area in front of the heat shield. The exact leakage mechanisms and the relative role of poloidal versus toroidal leakage is not yet known and will be investigated in a future publication. Therefore, using line-integrated H-alpha signals to measure the heat shield recycling flux, under the assumption that the majority of emission comes from local recycling, would result in a large overestimation of the heat shield recycling source.

Without the introduction of new viewing lines or spectroscopic diagnostics it may not be easily possible to measure the recycling on the heat shield. However, modeling of the standard magnetic field configuration showed that the majority of the heat shield recycling is expected to occur in one location, above the baffle near the high iota target. This location may provide a convenient avenue toward quantifying plasma-surface interaction and recycling fluxes on the heat shield in the experiment. The feasibility of measuring the particle source from this region using line integrated measurement should be tested in simulation in the future.

Full experimental reconstruction of the local recycling flux from individual components from H-alpha emission is extremely complex, particularly in regions of low expected recycling flux. At the moment, not enough information is known to localize the particle flux from the individual PFCs in the experiment. With the addition of the proposed viewing area on the heat shield above the high iota target to the current diagnostic line-up, full localized reconstructions with the aid of 3D modeling, such as described in [9], may be possible in the future.

Acknowledgments

Appendix

Git code versions for EMC3-EIRENE.
Git version for plasma background calculations (MPCDF Gitlab):
EMC3: 147b338402f9788703b84fc9a0c33e4425adf6f9
EIRENE: 0e5fd189824e47eb060f8e0317851181b496b3f7
Git version for post-processed H-alpha spectroscopic analysis (UW_fusion Gitlab):
EMC3: eb9f4d5d9e489e99e617b58e99e81f73d7db9a73

ORCID iDs

V R Winters ● https://orcid.org/0000-0001-8108-7774
F Reimold ● https://orcid.org/0000-0003-4251-7924
R König ● https://orcid.org/0000-0002-4772-0051
T Romba ● https://orcid.org/0000-0002-2727-9385
C Biedermann ● https://orcid.org/0000-0001-9318-7334
S Bozhenkov ● https://orcid.org/0000-0003-4289-3532
P Drewelow ● https://orcid.org/0000-0003-0121-9058
M Endler ● https://orcid.org/0000-0003-2314-8393
H Frerichs ● https://orcid.org/0000-0002-3527-5106
J Geiger ● https://orcid.org/0000-0003-4268-7480
Y Gao ● https://orcid.org/0000-0001-8576-0970
J H Harris ● https://orcid.org/0000-0003-4512-3621
M Jakubowski ● https://orcid.org/0000-0002-6557-3497
T Kremeyer ● https://orcid.org/0000-0002-6383-944X
H Niemann ● https://orcid.org/0000-0003-0300-1060
G Schlisio ● https://orcid.org/0000-0002-5430-0645
G A Wurden ● https://orcid.org/0000-0003-2991-1484

References

[1] Loarer T *et al* 2004 Overview of gas balance in plasma fusion devices *20th IAEA Fusion Energy Conf. Proc.* Villamoura, Portugal (Vienna: International Atomic Energy Agency) (https://inis.iaea.org/collection/NCLCollection Store/_Public/36/078/36078348.pdf)
[2] Jakubowski M *et al* 2018 *Rev. Sci. Instrum.* **89** 10E116
[3] Colchin R J, Hillis D L, Maingi R, Klepper C C and Brooks N 2003 *Rev. Sci. Instrum.* **74** 2068
[4] McNeill D H 1989 *J. Nucl. Mater.* **162–4** 476–91
[5] Brezinsek S *et al* 2005 *Plasma Phys. Control. Fusion* **47** 615–34
[6] Feng Y, Sardei F and Kisslinger J 1999 *J. Nucl. Mater.* **266–9** 812–18
[7] Feng Y *et al* 2014 *Contrib. Plasma Phys.* **54** 426–31
[8] Frerichs H *et al* 2016 *Rev. Sci. Instrum.* **87** 11D441
[9] Frerichs H *et al* 2017 *Nucl. Fusion* **57** 126022
[10] Dai S *et al* 2016 *Nucl. Fusion* **56** 066005
[11] Dai S *et al* 2018 *Nucl. Fusion* **58** 096024
[12] Kawamura G *et al* 2018 *Plasma Phys. Control. Fusion* **60** 054005
[13] Boscary J *et al* 2013 *Fusion Sci. Technol.* **64** 263–8
[14] Reiter D, Baelmans M and Boerner P 2005 *Fusion Sci. Technol.* **47** 172–86
[15] Sereda S *et al* 2020 *Nucl. Fusion* **60** 086007
[16] Lazerson S *et al* 2018 *Plasma Phys. Control. Fusion* **60** 124002
[17] Pasch E *et al* 2016 *Rev. Sci. Instrum.* **87** 11E729
[18] Stephey L *et al* 2016 *Rev. Sci. Instrum.* **87** 11D606
[19] The AMJUEL online database 2020 (available at: www.eirene.de/html/amjuel.html)
[20] Wenzel U *et al* 2019 *Rev. Sci. Instrum.* **90** 123507
[21] Feng Y *et al* 2016 *Nucl. Fusion* **56** 126011
[22] Ford O *et al* 2020 *Rev. Sci. Instrum.* **91** 023507
[23] Fujii K *et al* 2015 *Nucl. Fusion* **55** 063029